Complete transfer of populations from a single state to a pre-selected superposition of states using Piecewise Adiabatic Passage.

Evgeny A. Shapiro[1], Valery Milner[1,2,3], Moshe Shapiro[1,2,4]
Departments of Chemistry[1] and Physics & Astronomy[2],
and The Laboratory for Advanced Spectroscopy and Imaging Research (LASIR)[3],
The University of British Columbia, Vancouver, Canada,
[4]*Department of Chemical Physics, The Weizmann Institute, Rehovot, 76100, Israel,*
(Dated: March 1, 2009)

We develop a method for executing robust and selective transfer of populations between a single level and pre-selected superpositions of energy eigenstates. Viewed in the frequency domain, our method amounts to executing a series of simultaneous adiabatic passages into each component of the target superposition state. Viewed in the time domain, the method works by accumulating the wavefunction of the target wave packet as it revisits the Franck Condon region, in what amounts to an extension of the Piecewise Adiabatic Passage technique [Shapiro et.al., Phys. Rev. Lett. 99, 033002 (2007)] to the multi-state regime. The viability of the method is verified by performing numerical tests for the Na_2 molecule.

PACS numbers: 32.80.Qk,33.80.-b,42.50.Hz

I. INTRODUCTION

The availability of robust and selective methods of executing population transfers in multilevel quantum systems is essential for a variety of fields, such as precision spectroscopy [1, 2, 3, 4, 5], quantum computing [6, 7, 8, 9, 10, 11, 12], control of molecular dynamics and chemical reactions [13, 14, 15], production of cold molecules [16, 17, 18], biophotonics [19] and nanoscience [20, 21]. In this paper we propose a new method for transferring populations from a single energy eigenstate into a selected superposition of states (wave packet) using shaped broadband laser pulses. This simple method combines the robustness of adiabatic population passage [22, 23, 24] with the flexibility of femtosecond pulse shaping techniques [13, 14, 25, 26].

Our method is an integration of a number of earlier studies. Viewed in the frequency domain, it is an application of Coherently Controlled Adiabatic Passage (CCAP) [21, 27], which in itself is an extension of the three-state Stimulated Raman Adiabatic Passage (STIRAP) [24, 28, 29] and the adiabatic transfer between field-dressed states [30, 31, 32, 33, 34, 35] methods. The CCAP method presents a complete solution to the non-degenerate quantum control problem, i.e., the execution of a complete population transfer between superpositions (wave packets) of non-degenerate energy eigenstates.

Viewed in the time domain, the present method is an extension of Piecewise Adiabatic Passage [17, 36, 37] to the case of a target wave packet of states. In particular, when the spectrum of the target manifold is nearly harmonic, the driving field is given by a train of mutually coherent pulses separated by the evolution period of the target wave packet. Keeping the optical carrier phase of the pulses constant throughout the entire train of pulses results in the piecewise execution of periodic (Rabi) oscillations between the initial and the target states. The introduction of a "piecewise chirp", expressed as a pulse-to-pulse variation in the optical phase, is what eliminates the oscillations and renders adiabatic robustness to the population transfer.

Selectivity is obtained by tailoring the temporal and spectral profiles of the train of pulses to the attributes of the target wave packet dynamics [1, 38, 39, 40]. Such compatibility between the pulse train attributes and the target wave packet dynamics has also been noted in brute-force optimization studies [15, 41, 42] aimed at either maximizing population transfer into the target state [43, 44, 45] or stabilizing such transfer against wave packet spreading and decoherence [46].

The time profile of the field in our solution is reminiscent of the "multi-RAP" pulse sequences of Ref.[35]. As discussed below, the difference between the two solutions is manifest when the target wave packet consists of more than two eigenstates. Our method is also related to the coherent accumulation of transition amplitudes driven by a train of laser pulses [1, 4, 47, 48, 49, 50, 51, 52], but the robustness is a unique property of PAP.

This paper is organized as follows: In Section II, we present the theory in the frequency space and illustrate it via numerical studies of population transfer in sodium dimers. In Section III, we describe the population transfer in the time domain, and connect the two physical points of view. In Section IV, we establish numerically the accuracy of the method and its sensitivity to the pulse parameters. A discussion is provided in Section V.

II. MULTI-STATE ADIABATIC CHIRPING - FREQUENCY DOMAIN POINT OF VIEW.

In this section we extend the CCAP [21, 27] method of using a multi-mode pulse to execute wave packet adiabatic passage via an intermediate state to the chirped multi-mode pulse case. As in Refs.[21, 27], we consider a quantum system, initially in the ground state $|0\rangle$, coupled

by a laser field field $\epsilon(t)$, made up of N discrete modes, of frequencies ω_n, to a manifold composed of N excited states. Contrary to Refs. [21, 27] we allow the mode frequencies to slowly vary with time, hence we denote them as $\omega_n(t)$.

The material Hamiltonian is

$$\hat{H} = \hat{H}_M + \hat{\mu}\epsilon(t) = \hat{H}_M + 2f(t)\hat{\mu}\sum_{n=1}^{N}\epsilon_n \cos[\Phi_n(t)+\phi_n], \tag{1}$$

where $\hat{H}_M$ is the field-free Hamiltonian, $2f(t)\epsilon_n$ and ϕ_n are the mode amplitudes and phases, respectively. $\hat{\mu}$ is the dipole moment for the transition between the ground state and the manifold of excited states. We assume that each mode frequency $\omega_n(t) = \dot{\Phi}_n(t)$ is detuned by a small amount $\Delta_n(t) \equiv E_n - E_0 - \omega_n(t)$ with respect to one of the excited levels (denoted n), where E_0 and E_n are the field-free energies of the states $|0\rangle$ and $|n\rangle$, respectively,

$$(E_0 - \hat{H}_M)|0\rangle = (E_n - \hat{H}_M)|n\rangle = 0\ . \tag{2}$$

The material wave function expressed in a.u. ($\hbar = 1$) is expanded as

$$|\Psi(t)\rangle = b_0(t)e^{-iE_0t}|0\rangle + \sum_{n=1}^{N} b_n(t)e^{-i(E_0t+\Phi_n(t))}|n\rangle\ . \tag{3}$$

It is instructive to study the dynamics arising from the application of the Rotating Wave Approximation (RWA) [13, 14, 23, 24]. To do so we first average the non-stationary Schrödinger equation over time scales of the order of $1/\omega_n$, resulting in

$$\begin{aligned} i\,\dot{b}_0(t) &= f(t)\sum_{n=1}^{N} b_n(t)\mu_{0n}\sum_{l=1}^{N}\epsilon_l e^{i((\omega_l-\omega_n)t+\phi_l)}\ , \qquad (4)\\ i\,\dot{b}_n(t) &= \Delta(t)b_n(t) + f(t)b_0(t)\mu_{n0}\sum_{l=1}^{N}\epsilon_l e^{i((\omega_n-\omega_l)t-\phi_l)}. \end{aligned}$$

We also assume that each transition is driven by only one of the field modes - the mode with the smallest $\Delta_n(t)$ detuning. Denoting by $\Omega_n(t) \equiv f(t)\epsilon_n\mu_{n0}\,e^{-i\,\phi_n}$ the (complex) Rabi frequencies, and by $\mathbf{b}(t) = (b_0(t), b_1(t)...b_n(t))^{\mathsf{T}}$, the (column) vector of expansion coefficients, with the superscript T marking the "transpose" operation, we can now write the Schrödinger equation in matrix form as

$$i\,\dot{\mathbf{b}} = \mathrm{H}\mathbf{b}\ , \tag{5}$$

where

$$\mathrm{H}(t) = \begin{pmatrix} 0 & \Omega_1^*(t) & \dots & \Omega_N^*(t) \\ \Omega_1(t) & \Delta_1(t) & \dots & 0 \\ \vdots & \vdots & \ddots & \vdots \\ \Omega_N(t) & 0 & \dots & \Delta_N(t) \end{pmatrix}\ . \tag{6}$$

While the first part of the RWA (Eq.(4)) amounts to neglecting the terms which oscillate at optical frequencies, the second part (Eqs.(5,6)) is equivalent to averaging the Schrödinger equation over time scales of the order of $1/(\omega_n - \omega_m)$, resulting in loss of information about times scales shorter than a vibrational period. Nevertheless, the time-averaged Schrödinger equation (5) provides an accurate description of the wave function at the end of the process, after many vibrational periods. We postpone the study of the dynamics on a finer time scale to the following sections.

We now tune the chirping of the mode frequencies such that all the detunings are equal to one another, i.e., $\Delta_n(t) = \Delta(t)$. This allows us to easily diagonalize H at any given moment of time, obtaining $N-1$ degenerate "dark" eigenstates whose (quasi-) energies are equal to $\Delta(t)$, and two "bright" eigenstates whose eigenvalues are,

$$\lambda_\pm(t) = \Delta(t)/2 \pm \{\Delta^2(t)/4 + \Omega_{\rm eff}^2(t)\}^{\frac{1}{2}} \tag{7}$$

where $\Omega_{\rm eff}^2(t) = \sum_{n=1}^{N}|\Omega_n(t)|^2$. The eigenvectors corresponding to the bright solutions are

$$\mathbf{b}_\pm = \cos\theta_\pm \mathbf{b}_i + \sin\theta_\pm \mathbf{b}_f\ , \tag{8}$$

where

$$\mathbf{b}_i = (1,0,\dots,0)^{\mathsf{T}} \quad \mathbf{b}_f = (0,\Omega_1,\dots,\Omega_N)^{\mathsf{T}}/\Omega_{\rm eff}\ , \tag{9}$$

with $\tan\theta_\pm = \lambda_\pm/\Omega_{\rm eff}$. Note that each Ω_n, as well as $\Omega_{\rm eff}$, depends on time via the common factor $f(t)$. Therefore the definition of $\mathbf{b}_f$ in Eq.(9) is time independent. Further, $\tan\theta_+ \cdot \tan\theta_- = -1$, and $\lambda_- < 0$, hence,

$$\sin\theta_+ = \cos\theta_-, \qquad \cos\theta_+ = -\sin\theta_-\ . \tag{10}$$

If at some instant $|\Delta(t)| \gg \Omega_{\rm eff}(t)$, then one of the states represented by the $\mathbf{b}_+$ or $\mathbf{b}_-$ vector coincides with the $|\,i\,\rangle$ state, represented by the $\mathbf{b}_i$ vector, and the other - by the $|\,f\,\rangle$ state, represented by the $\mathbf{b}_f$ vector.

Similar to the textbook case of adiabatic following in a two-level system [23], when $\Delta(t)$ is made to vary slowly enough, the system makes a smooth transition from state $|\,i\,\rangle$ to state $|\,f\,\rangle$. We show in the Appendix that there are no transitions between the $|\pm\rangle$ bright eigenstates and the dark states. As a result, the dark states remain unpopulated at all times. Hence it is possible to make the adiabatic population transfer complete, provided that the bandwidth of the pulse covers the whole range of the target energies E_n.

In order to create the required field, one can start with a single broadband laser pulse, and spectrally shape it in the way illustrated in Fig. 1(a). Here, the field is frequency chirped in the neighborhood of each resonance frequency $\omega_n^{res} = (E_n - E_0)$, according to,

$$\epsilon(\omega) = \epsilon_n\, F(\omega - \omega_n^{res})\, e^{i\,\alpha_\omega(\omega-\omega_n^{res})^2/2}\, e^{i(\omega t_0 - \phi_n)}\ . \tag{11}$$

The real amplitude envelope $F(\omega)$ reaches its maximum of 1 at $\omega = 0$ and serves to suppress the pulse spectrum

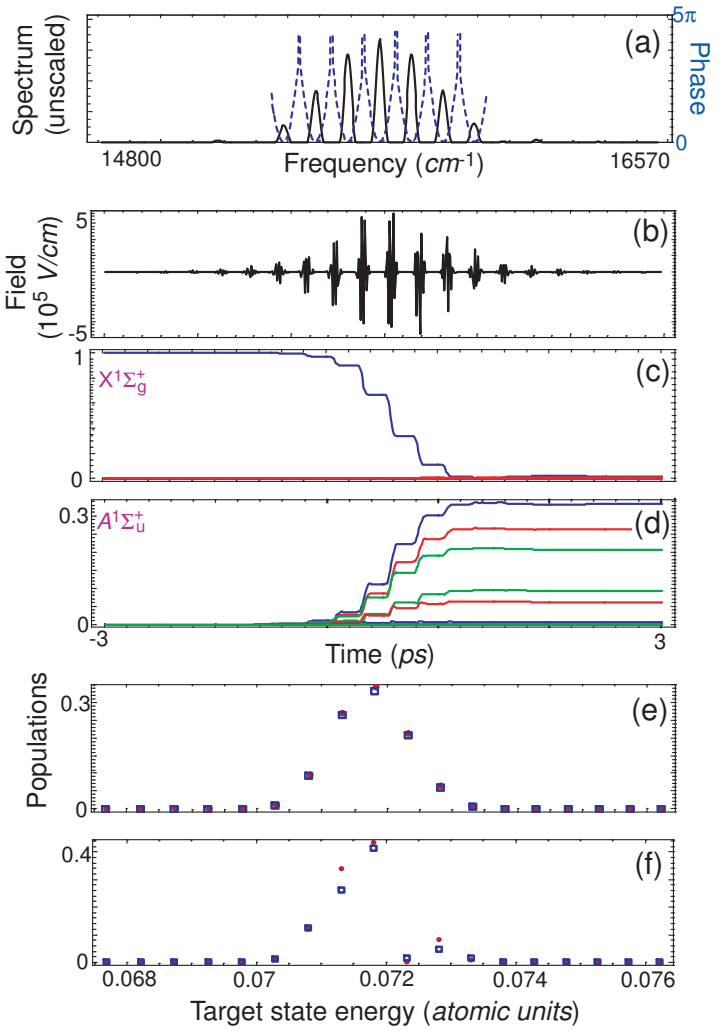

FIG. 1: (Color online) Piecewise adiabatic following in Na_2. (a): Amplitude spectrum (solid black) and frequency-dependent phase (dashed blue) of the driving field. (b): The driving field as a function of time. (c,d): Populations of various vibrational levels of the ground and excited electronic states. (e): Final populations of $A^1\Sigma_u^+$ states predicted by the theory (full red circles), and obtained in the numerical simulation (empty blue squares).(f): Same as (e) for the case when the spectral region corresponding to the transition into one of the excited levels is blocked.

between the resonance regions. The requirements for this suppression will be discussed in Section IV. For Gaussian profile of the field envelope near each ω_n^{res},

$$F(\omega-\omega_n^{res}) = \exp\left[(\omega-\omega_n^{res})^2/2\sigma_\omega^2\right] \ . \qquad (12)$$

The above form corresponds to the field parameters of Eq. (1) assuming the form,

$$\begin{aligned}
\Phi_n(t) &= \omega_n^{res}(t-t_0) + \frac{\alpha_t}{2}(t-t_0)^2 + \phi_c, \\
f(t) &= \frac{\sigma_w(2\pi)^{\frac{1}{2}}}{(1+\alpha_\omega^2\sigma_\omega^4)^{\frac{1}{4}}} \exp\left[-(t-t_0)^2/2\sigma_t^2\right], \\
\phi_c &= -\arg\left[1-i\alpha_\omega\sigma_\omega^2\right]/2, \qquad (13) \\
\sigma_t^2 &= (1+\alpha_\omega^2\sigma_\omega^4)/\sigma_\omega^2 \ , \\
\alpha_t &= \alpha_\omega\sigma_\omega^4/(1+\alpha_\omega^2\sigma_\omega^4) \ .
\end{aligned}$$

In the adiabatic transfer into a pre-selected superposition state, the real amplitudes $\epsilon_n = \epsilon(\omega_n^{res})$ and phases ϕ_n are chosen such that the vector $\mathbf{b}_f$ given by Equation (9) represents the $|\,f\,\rangle$ target state. The direct correspondence between Eqs.(7,8) and the equations describing adiabatic following in a two-level system driven by a single-component chirped pulse [23] suggests that the variation of each chirped resonant frequency must exceed $\Omega_{\rm eff}$.

Fig. 1 shows a simulation of the adiabatic transfer between the $v = 0$ vibrational state of the $Na_2(X^1\Sigma_g^+)$ ground electronic state, and a vibrational wave packet composed of the $v = 7,..,12$ states of the $A^1\Sigma_u^+$ state [53]. In order to assess the fidelity of the transfer we have also computed the population of neighboring $X^1\Sigma_g^+$ and $A^1\Sigma_u^+$ vibrational levels. Panel (a) shows a field spectrum obtained by frequency modulating a $\sin^2\beta t$-type pulse. The pulse duration is 55fs and its central wavelength is 638 nm, with chirp parameter $\alpha_\omega = 2\times10^5 \mathrm{fs}^2$. As discussed in detail in the next section, the piecewise chirped pulse of panel (a) corresponds in the time domain to the train of pulses shown in Fig. 1(b).

In Fig. 1(c-e) we display the dynamics of the population transfer. As demonstrated in Fig. 1(e), the populations of the target wave packet energy components practically coincide with the predictions of Eq.(9). In Fig. 1(f) we demonstrate the selectivity of the method by changing the amplitudes ϵ_n and the phases ϕ_n characterizing the field components. In each case, the distribution of the final populations in the target manifold remains close to that predicted by Eq.(9), though the component phases could at times deviate from the target ones, somewhat lowering the magnitude of the overlap with the target wave packet to $\sim 0.8-0.95$. This point is discussed further in section IV.

The mechanism of the population transfer becomes transparent if the laser field is represented by a phase-space (Husimi) spectrogram. Fig. 2(a) shows the spectrogram of the field of Fig. 1(a,b). Each point displays the absolute value of the overlap integral of the field with a Gaussian probe pulse,

$$\epsilon^{(p)}(t) = \exp\left[-\frac{1}{2}\left(\frac{t-t_0^{(p)}}{\sigma_t^{(p)}}\right)^2 - i\omega^{(p)}t + i(\omega^{(p)}-\omega_0)t_0^{(p)}\right] \qquad (14)$$

of long duration ($\sigma_t^{(p)} = 1000$ fs). The frequency and time axes correspond to $\omega^{(p)}$ and $t_0^{(p)}$, respectively. It is clear that the field drives a number of adiabatic passages simultaneously: An adiabatic transition into n^{th} excited level may occur when the instantaneous frequency component ω_n crosses the n^{th} resonance at $\omega_n^{res} = E_n - E_0$.

The mechanism displayed here is quite different from that of the "molecular π-pulse" [54, 55, 56, 57, 58], where a transition into the manifold of excited states is driven by a single frequency-chirped laser field. While in the scheme proposed here all the transitions take place simultaneously, in the case of a molecular π-pulse the energy of the initial state shifted by the energy of one photon, $[E_0 + \omega(t)]$, crosses all the target energies one by one. As a result, the system passes through a chain of avoided crossings. This is illustrated in Fig. 2(b) which shows the spectrogram ($\sigma_t^{(p)} = 200$fs) of the molecular π-pulse obtained from the original un-shaped field, used in our numerical examples, by applying a single frequency chirp of $\alpha_\omega = 2 \times 10^4$ fs^2. Although a molecular π-pulse can transfer all the initial population into the excited manifold in a robust way, the relative amplitudes of the states in the resulting wave packet are not controllable unless the target manifold consists of only two states. In the latter case, employing either up- or down- frequency chirp allows population transfer in either the lower or the higher eigenstate of the target manifold [34]. We refer the reader to Ref.[58] for a detailed analysis of the population transfer by molecular π-pulses.

The question of selectivity also arises when comparing our method to the family of Stark-assisted adiabatic transfers [59], and the transfer via multiple successive Rapid Adiabatic Passages [35]. While in both examples the possibility of robust and selective transfer into either one of the two target states has been found, it is not clear whether these methods can enable population transfer into a selected superposition of target states, especially if $N > 2$.

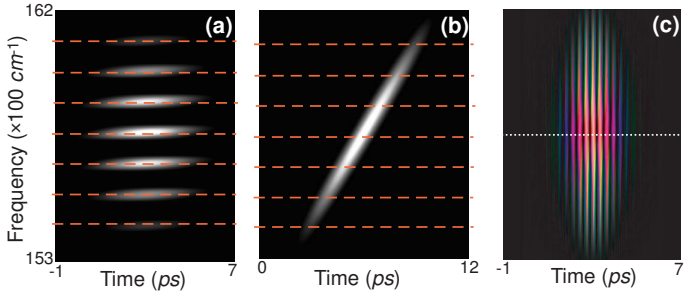

FIG. 2: (Color online) Field spectrograms. (a): Absolute values of the overlap integral of the pulse train field with probe Gaussian pulses. The red horizontal lines show the resonance frequencies ω_n^{res}. (b): Spectrogram of a conventional frequency-chirped pulse. (c): Expansion of the pulse train field in short probe pulses. The amplitude of each projection is shown by brightness, its phase by color. The white dotted line marks the spectral center of the pulse.

III. MULTI-STATE ADIABATIC CHIRPING - TEMPORAL POINT OF VIEW.

In order to understand the dynamics of the population transfer on a finer time scale, here we develop the time-domain description of the process. Fig. 1(b) shows the time-dependent driving field of the above example. The time analogue of Eq.(11) is

$$\epsilon(t) = R_e\, f(t) \exp\left[i\omega_0(t-t_0) + i\alpha_t(t-t_0)^2/2 + i\phi_c\right] g_1(t) \tag{15}$$

where $\omega_0 = \omega_{n_0}^{res}$ is chosen to coincide with the frequency of a transition into one of the central states $|n_0\rangle$ of the excited wave packet, and

$$g_1(t) = 2\sum_{n=1}^{N} \epsilon_n \exp\left[i(E_n - E_{n_0})(t-t_0) + i\phi_n\right] \ . \tag{16}$$

Equation (16) is similar to an expression describing wave function dynamics of a fictitious wave packet in the target manifold, with the amplitudes of eigenstates given by $\epsilon_n \exp[i\phi_n]$. If the target spectrum and the distribution of the complex field amplitudes $\epsilon_n \exp[i\phi_n]$ are both smooth, then the interference between the different frequency components of the field results in a train of short pulses separated by the vibrational period $T_{vib} = dE_n/dn$ of the target wave packet. The field pattern is restored whenever $(E_n - E_{n_0})t \simeq 2\pi m$ for all n and any integer m. Such a train of short pulses is seen in Fig. 1(b). Further, if the target spectrum is harmonic, then the field spectrum is a frequency comb with equally spaced teeth, and the pulse shape is preserved within the train. If the spectrum is anharmonic, then the shape evolves from pulse to pulse within the train, reflecting the spreading of the target wave packet as it revisits the transition region.

When the target spectrum is weakly anharmonic, the pulse train of Eq. (15) is composed of pulses which differ from one another in four essential ways: First, the temporal spacings between the adjacent pulses (which may have different overall power) change. Second, their central frequencies differ by $\alpha_t\, T_{vib}$. Third, and most important, the l^{th} pulse has an extra overall phase equal to $\alpha_t\,(lT_{vib})^2/2$, where $l = 0$ corresponds to the middle of the pulse train; and fourth, owing to the anharmonicity, the condition $(E_n - E_{n_0})t = 2\pi m$ is fulfilled for different n at slightly different times, leading to change in the pulse duration from pulse to pulse.

Fig. 2(c) shows the spectrogram of the field of Fig. 1(a,b) using short ($\sigma_t^{(p)} = 50$fs) probe pulses, whose exact form is given by Eq. (14). Naturally, the representation in terms of short probe pulses gains temporal resolution but loses frequency resolution. The optical phase of the short pulses within the train varies quadratically with the pulse number. This is displayed in Fig. 2(c) by the variation in color along the central-frequency section, from orange (phase equal to zero) in the middle of the train, to purple and blue, and finally to green (phase $\simeq 3\pi/2$), at the very tails. Note that the pulse-

to-pulse drift of the central frequency is not noticeable on the scale of the figure.

The field in the above example is similar to that introduced in Ref.[37] for the piecewise adiabatic passage in a two-level system. This is readily seen both in the frequency-domain representation (by comparing Fig.1(a) with Fig.3(b) of Ref.[37]), and in the time-domain representation. The almost-periodic pulse train only drives transitions between the $|\,i\,\rangle$ and $|\,f\,\rangle$ states. The train of short pulses, tailored to fit the periodic evolution of the $|\,f\,\rangle$ state, peaks every time this state revisits the Franck-Condon region. At these instants a superposition state $|\,\psi\,\rangle$ can be represented by the unit Bloch vector of Fig. 3, defined by the θ and ϕ angles,

$$|\,\psi\,\rangle = \cos(\theta/2)|i\rangle + \sin(\theta/2)e^{i\phi}|f\rangle\ , \qquad (17)$$

The present 1+many-level system differs from the two level system in a fundamental way, since here the relative phases of the components of the target wave packet change all the time. There are points of similarity as well, because here too, the process can be depicted, as shown in Fig. 3, by the discontinuous motion of a unit vector on a ("Bloch") sphere, with the polar angle $\theta = 0$ representing $|\,i\,\rangle$ and $\theta = \pi$ representing $|f\rangle$. The effect of each pulse (of short duration τ) is now viewed as a rotation $\hat{P} \equiv \mathrm{R}(\alpha_P)$ of the Bloch vector by an angle $\alpha_P = \int_\tau \Omega_{\rm eff}(t)dt$ about the y axis. The change in the carrier phase between consecutive pulses can be represented by an additional rotation about the z axis, $\hat{F} \equiv \mathrm{R}_z(\alpha_F)$. Thus, the overall evolution due to the pulse train of Eq. (15) is represented by a sequence $\hat{U} = ...\hat{T}\hat{F}\hat{P}\hat{T}\hat{F}\hat{P}...$,. The operator $\hat{T}$, which corresponds to the free evolution of the wave packet between pulses, keeps the Bloch vector orientation at the beginning of each short pulse in the train equal to that at the end of the previous one.

The product $\hat{F}\hat{P}$ of two rotations can be viewed as an overall rotation by an angle α_0 about an instantaneous axis defined by the (θ_0, ϕ_0) angles, given to lowest-order expansion in α_P, α_F as

$$\alpha_0 = \{({\alpha_P}^2 + {\alpha_F}^2)/2\}^{\frac{1}{2}}, \qquad \phi_0 = \pm\pi/2 - \alpha_F/2,$$

$$\tan\theta_0 = \pm\alpha_P/\alpha_F. \qquad (18)$$

By maintaining the same value of α_F and α_P throughout the pulse train we can induce piecewise rotations of the Bloch vector about the "adiabatic" trajectory traced out by (θ_0, ϕ_0). As shown in Fig. 3, by slowly varying the values of α_P, α_F we can make the Bloch vector follow this adiabatic trajectory. Such piecewise following can be realized provided, (i) the y- and z-rotations are small (i.e. each pulse should induce an angular change much smaller than π and each increment in the carrier phase should be small too); (ii) (θ_0, ϕ_0) should not move much from pulse to pulse, i.e.

$$\Delta\theta_0 \ll \{({\alpha_P}^2 + {\alpha_F}^2)/2\}^{\frac{1}{2}}. \qquad (19)$$

In the pulse train of Eq. (15), initially $\alpha_P \ll |\alpha_F|$: $\Omega_{\rm eff}$ is small, while the pulse-to-pulse phase change is significant. As α_P increases and $|\alpha_F|$ decreases, the states originating in $|i\rangle$ and $|f\rangle$ move towards the equator of the Bloch sphere. They cross the equator as soon as α_F changes sign, and finally interchange with each other. Depicted in the original non-rotated frame, the trajectory of the Bloch vector is a piecewise spiral, similar to that shown in Fig.3.

IV. NUMERICAL STUDIES.

Fig. 4 shows the population transferred into the target manifold, and the projection of the final state onto the target wave packet comprised of vibrational eigenstates of Na_2 in the $A^1\Sigma_u^+$ electronic state as a function of the chirp α_ω and the field strength ϵ^0 of the original 55fs pulse used in the computations presented in Fig. 1. The plots reveal several interesting features. First, for both positive and negative chirps exceeding in magnitude $|\alpha_\omega| \sim 200000\mathrm{fs}^2$, the transfer is almost complete and quite robust with respect to changing α_ω and ϵ^0. For a large range of pulse parameters the transfer probability is $\sim 95\%$, and the projection of the final state onto the target is $\sim 0.85 - 0.9$.

The transfer probability landscape at small values of α_ω corresponds to the piecewise Rabi oscillations between the initial state and the excited wave packet. A close look at the population dynamics in this region of parameter space shows that the first few pulses in the train manage to completely empty state $|0\rangle$, while the following pulses re-populate it. At stronger fields, state $|0\rangle$ is de-populated and re-populated several times during the pulse sequence. Populations of the nearby vibrational eigenstates of the $X^1\Sigma_g^+$ manifold remain negligible at all times, with the ratios of populations of different $A^1\Sigma_u^+$

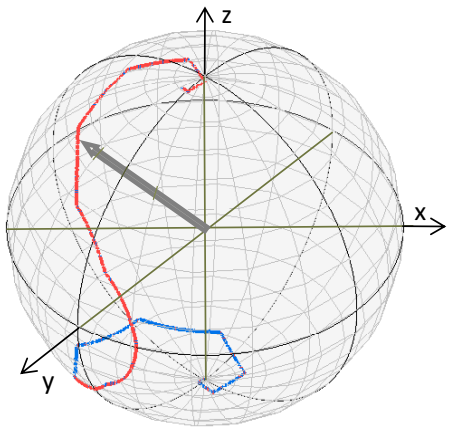

FIG. 3: (Color online). A calculated sample trajectory of the Bloch vector (thick gray arrow) during the a piecewise AP process implemented with a train of 20 ultra-short pulses [37].

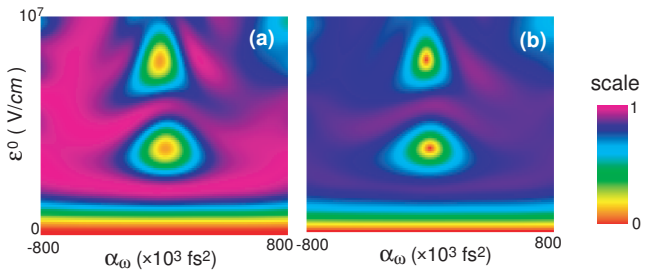

FIG. 4: (Color online) Population transferred into the target manifold (a), and the projection on the target wave packet (b) as a function of the chirp α_ω and field strength ϵ^0.

states remaining close to the target values.

We also note that though the parameter-space region where robust population transfer occurs includes pulse areas of $\sim \pi$, the optimal pulses have areas larger than π. The pulse area cannot be increased beyond a certain value because when individual pulses within the pulse train are able to drive a significant population transfer, condition (i) above breaks down, and the overall fidelity decreases.

The fidelity profile of Fig. 4 is quite robust with respect to changes in the spectral width σ_ω in the vicinity of each resonance frequency ω_n^{res}. However, when σ_ω approaches half of the distance between the neighboring resonance frequencies, the transfer fidelity exhibits ripples as a function of α_ω, eventually becoming unstable. Indeed, for the Gaussian amplitude modulation of the spectrum (Eq.(12-13)), and assuming that the chirp is strong so that $\alpha_\omega \sigma_\omega^2 \gg 1$, one has

$$\sigma_t = \alpha_\omega \sigma_\omega, \qquad \alpha_t = 1/\alpha_\omega \ , \tag{20}$$

and the instantaneous frequency of the $n^{\rm th}$ component of the field at the end of the pulse train becomes

$$\omega_n(t = t_0 + 2\sigma_t)\ \omega_n^{res} + 2\sigma_t \alpha_t \simeq \omega_n^{res} + 2\sigma_w \ . \tag{21}$$

If $\sigma_\omega \geq (\omega_{n+1}^{res} - \omega_n^{res})/2$ then the instantaneous frequency of the $n^{\rm th}$ field component at the end of the pulse train coincides with the adjacent resonance. In this case the dynamics can not be viewed as a set of independent parallel adiabatic passages into different target states.

V. SUMMARY AND DISCUSSION.

In this paper we have developed a method for executing robust and selective transfer of population from a single energy eigenstate to a pre-selected superposition of energy eigenstates. Viewed in the frequency domain, the method constitutes simultaneous transfer of population to all the energy eigenstates which make up the superposition state by a set of parallel adiabatic passages. Viewed from the time domain, the method amounts to using a train of pulses to accumulate wavelets which make up the target wave packet as it revisits the Franck Condon region [18, 36, 37].

We have tested the method numerically by simulating transitions between a single vibrational eigenstate and a superposition of vibrational energy eigenstates of Na_2 in the $A^1\Sigma_u^+$ state. The simulations confirmed the high selectivity and robustness of the method.

Topics to be investigated further include: An accurate description of the transfer dynamics for a general anharmonic spectrum and in particular the description of the short-time dynamics of the transfer. This may be achieved using Floquet states [31, 32] dressed by a multimode driving field. Also, although the present theory is quite accurate in predicting the ratio of populations transferred into the target wave packet, the reasons for the phase errors, resulting in less than perfect overlap with the target state, need to be investigated.

Acknowledgments

This work was supported by grants from CFI, BCKDF and NSERC.

VI. APPENDIX: PROOF THAT THE DARK STATES REMAIN UNPOPULATED.

This proof follows Ref.[21], where similar arguments were made in the context of CCAP. These arguments were based on the standard treatment of adiabatic transfer [13, 22, 23].

It follows from Eq.(6) that each dark state is described at a given time by the vector of amplitudes $\mathbf{b}_{dark} = (0, b_{1\perp}, ..., b_{N\perp})^{\mathsf{T}}$ which is orthogonal to both $\mathbf{b}_i = (1, 0, ...0)^{\mathsf{T}}$ and $\mathbf{b}_f = (0, \Omega_1/\Omega_{\rm eff}, ..., \Omega_N/\Omega_{\rm eff})^{\mathsf{T}}$. Since the mutual ratio of different Rabi frequencies Ω_n does not change in time, we can choose for the dark states an $N-1$-dimensional time-independent basis $(0, e_{1\perp}^{(n)}, ..., e_{N\perp}^{(n)})^{\mathsf{T}}$, $n = 1..N-1$. Introducing the vector $\mathbf{a}$ of amplitudes of instantaneous eigenstates,

$$\mathbf{b}(t) = \mathrm{U}(t)\mathbf{a}(t) \ , \tag{22}$$

where the columns of U are given by the normalized eigenvectors of H, and using the relation $\mathrm{U}^\dagger \mathrm{U} = 1$, we have that

$$i\,\dot{\mathbf{a}} = \mathrm{U}^\dagger \mathrm{H} \mathrm{U}\,\mathbf{a} - i\,\mathrm{U}^+ \dot{\mathrm{U}}\,\mathbf{a} \ . \tag{23}$$

The first term on the right-hand side of Eq.(23) governs the adiabatic evolution. The second term governs nonadiabatic transitions between the instantaneous eigenstates. Let us choose the order of adiabatic eigenvalues such that the adiabatic Hamiltonian $\mathrm{U}^\dagger \mathrm{H} \mathrm{U}$ has on its main diagonal $(\lambda_+, \lambda_-, \Delta, ...\Delta)$, with $N-1$ terms equal to Δ, and all the off-diagonal elements equal to zero. Then, using Eq.(10), we obtain

$$\mathrm{U} = \begin{pmatrix} \cos\theta_+ & \sin\theta_+ & 0 & \dots & 0 \\ \sin\theta_+\,\Omega_1/\Omega_{\rm eff} & -\cos\theta_+\,\Omega_1/\Omega_{\rm eff} & e_{1\perp}^{(1)} & \dots & e_{1\perp}^{(N-1)} \\ \vdots & \vdots & \vdots & \ddots & \vdots \\ \sin\theta_+\,\Omega_N/\Omega_{\rm eff} & -\cos\theta_+\,\Omega_N/\Omega_{\rm eff} & e_{N\perp}^{(1)} & \dots & e_{N\perp}^{(N-1)}. \end{pmatrix} \tag{24}$$

As a result of the above structure of U, the non-adiabatic matrix is given as,

$$\mathrm{U}^\dagger\dot{\mathrm{U}} = \begin{pmatrix} 0 & \dot\theta & \mathbf{0} \\ -\dot\theta & 0 & \\ \mathbf{0} & & \mathbf{0} \end{pmatrix}. \tag{25}$$

We see that this matrix does not couple the bright and dark states. Hence the $N-1$ dark states remain unpopulated at all times.

[1] L. Dhar, J.A. Rojers, K.A. Nelson, Chem. Rev. **94**, 157 (1994).
[2] A. Stolow, Phil. Trans. Roy. Soc. A **356** 345 (1998).
[3] S. A. Diddams *et al.*, Scie nce **306**, 1318 (2004).
[4] M.C. Stowe *et. al.*, Adv. At. Mol. Opt. Phys. **55**, 1 (2007); M.C. Stowe *et. al.*, Phys. Rev. Lett **96**, 153001 (2006).
[5] *Femtosecond optical frequency comb technology: principle, operation, and applications*, edited by J. Ye and S.T. Cundiff (Springer, New York, 2005).
[6] T.C. Weinacht, J. Ahn, P.H. Bucksbaum, Nature, **397**, 233 (1999).
[7] M. D. Lukin, *et. al.*Phys. Rev. Lett. **87** 037901 (2001).
[8] C.M. Tesch, R. de Vivie-Riedle, Phys. Rev. Lett. **89**, 157901 (2002);
[9] J.P. Palao, R. Kosloff, Phys. Rev. Lett. **89**, 188301 (2002).
[10] A. Muthukrishnan, C.R. Stroud, Jr, Phys. Rev. A, **62**(5), 052309 (2000).
[11] Z. Amitay, R. Kosloff, S.R. Leone, Chem. Phys. Lett. **359**, 8 (2002).
[12] E.A. Shapiro, M. Spanner, M.Yu. Ivanov, Phys. Rev. Lett. **91** 237901 (2003).
[13] M. Shapiro and P. Brumer, *Principles of the Quantum Control of Molecular Processes* (Wiley-Interscience, Hoboken, N.J., 2003).
[14] S.A. Rice, M. Zhao, *Optical control of molecular dynamics* (John Wiley & Sons, New York, 2000).
[15] H. Rabitz, R. de Vivie-Riedle, M. Motzkus, K. Kompa, Science **288**, 824 (2000)
[16] J. Doyle *et. al.*, European Physical Journal D **31**, 149 (2004), and references therein.
[17] A. Pe'er *et. al.*, Phys. Rev. Lett. **98**, 113004 (2007);
[18] E. A. Shapiro *et al.*, arXiv:0710.5502v1 [quant-ph] (2007).
[19] S. A. Malinovskaya, V. S. Malinovsky, Opt. Lett. **32**, 707 (2007);
[20] Special issue "Light control at the nanoscale", P. Kral and M. Shapiro, eds. J. Phys. B **40**(11) (2007).
[21] P. Kral, I. Thanopulos, and M. Shapiro, Rev. Mod. Phys. **79**, 53 (2007), and references therein.
[22] A. Messiah, *"Quantum Mechanics"* (Dover Publications, New York, 1999).
[23] L. Allen and J. H. Eberly, *Optical Resonance and Two-Level Atoms* (Wiley, New York, 1975).
[24] N. V. Vitanov *et al.*, Adv. At. Mol. Opt. Phys. **46**, 57 (2001).
[25] A. M. Weiner, Rev. Sci. Instrum. **71**, 1929 (2000).
[26] M. Dantus and V.V. Lozovoy, Chem. Rev. **104** 1813 (2004).
[27] I. Thanopulos and Moshe Shapiro, Phys. Rev. A **74**, 031401(R) (2006).
[28] J. Oreg, F.T. Hioe, J.H. Eberly, Phys. Rev. A **29**, 690 (1984).
[29] U. Gaubatz *et. al.*, J. Chem. Phys. **92**, 5363 (1990);
[30] J.H. Shirley, Phys. Rev., **138**(4B), B979-B987 (1965); B.Ya. Zeldovich, Zh. Exp. Theor. Fiz. **51**, 1493 (1966); V.I. Ritus, Zh. Exp. Theor. Fiz. **51**, 1544 (1966)
[31] S. Guérin, H.R. Jauslin, Eur. Phys. J. D **2**, 99 (1989).
[32] K. Drese and M. Holthaus, Eur. Phys. J. D **5**, 119 (1999).
[33] G.N. Gibson, Phys. Rev. A **72** 041404(R) (2005).
[34] M. Wollenhaupt *et al.*, App. Phys. B **82**, 183 (2006).
[35] T. Bayer, M. Wallenhaupt, T. Baumert, J. Phys. B **41** 074007 (2008).
[36] E. A. Shapiro *et al.*, Phys. Rev. Lett. **99**, 033002 (2007).
[37] S.Zhdanovich *et.al.*, Phys. Rev. Lett. **100**, 103004 (2008).
[38] L.E.E. deAraujo, I. Walmsley, C.R. Stroud, Jr, Phys. Rev. Lett. **81**, 955 (1998);
[39] M. Wollenhaupt *et al.*, Phys. Rev. A **73**, 063409 (2006).
[40] L. E.E. de Araujo,Phys. Rev. A **77**, 033419 (2008)
[41] R. S. Judson, H. Rabitz, Phys. Rev. Lett. **68**, 1500 (1992).
[42] V.S. Malinovsky, C. Meier, D. Tannor, Chem. Phys. **221**, 67 (1997).
[43] S. Grafe, C. Meier, V. Engel, J. Chem. Phys. **122**, 184104 (2005).
[44] C. Trallero-Herrero, J. L. Cohen, and T. Weinacht, Phys. Rev. Lett. **96**, 063603 (2006).
[45] T. Laarmann, I. Shchatsinin, P. Singh, N. Zhavoronkov, C.P. Schulz I.V. Hertel, J. Phys. B **41**, 074005 (2008).
[46] M.P.A. Branderhorst et. al., Science **320** 638 (2008).
[47] J.-C. Diels, S. Besnaiou, J. Chem. Phys. **85**, 6347 (1986).
[48] R.J. Temkin, J. Opt. Soc. Am. **10**, 830 (1993).
[49] N.V. Vitanov, P.L. Knight, Phys. Rev. A **52**, 2245 (1995).
[50] D. Felinto, C.A.C. Bosco, L.H. Acioli, S.S. Vianna, Opt.

Commun. **215**, 69 (2003).
[51] N. Dudovich *et al.*, Phys. Rev. Lett. **94**, 083002 (2005).
[52] M. Seidl, C. Uiberacker, W. Jakubetz, Chem. Phys. **349**, 296 (2008).
[53] The molecular potentials were modeled as those of Morse oscillators, with the data taken from NIST Chemistry WebBook, http://webbook.nist.gov/, accessed in December 2007. The electronic transition dipole between the $X^1\Sigma_g^+$ and $A^1\Sigma_u^+$ states was set equal to 4 atomic units.
[54] J. Cao, C. J. Bardeen, and K. R. Wilson, Phys. Rev. Lett. **80**, 1406 (1998).
[55] V.V. Yakovlev, C.J. Bardeen, J.Che, J. Cao, K.R. Wilson,J. Chem. Phys. **108**, 2309 (1998);
[56] C.J. Bardeen, Q. Wang, C.V. Shank, J. Phys. Chem. A **102**, 2759 (1998);
[57] C.J. Bardeen, V.V. Yakovlev, J. Che, J.A. Squier, K.R. Wilson, J. Am. Chem. Soc. **120** 13023 (1998).
[58] V. S. Malinovsky and J. L. Krause, Phys. Rev. A **63**, 043415 (2001).
[59] B.Y. Chang *et. al.*, Phys. Rev. A **75** 063405 (2007).